Projective calibration of a laser 3D scanner using the complete quadrangle*

Josep Forest[a], Joaquim Salvi[a], Enric Cabruja[b], Marc Bigas[b]

[a]Institut d'Informàtica i Aplicacions, Universitat de Girona, Campus Montilivi, Girona, Catalonia;

[b]Centre Nacional de Microelectrònica, Campus Bellaterra, Barcelona, Catalonia

ABSTRACT

Three-dimensional scanners are used for measurement purposes. They measure shapes by acquiring (or digitising) a set of points, commonly referred to as a *cloud of points*, which is a discrete approximation of a real object. Obviously, the dimensions of the digital representation should be as close as possible to the dimensions of the real object. One of the very well known quantities used in any metric measurement process is *accuracy*, which is defined as the maximum radius of the sphere inside which there is total probability of finding the coordinates of a measured point. From the above definition, it is clear that the smaller this radius is, the better the approximation of the reconstruction to the real object will be. The key factors for maximising accuracy are essentially the method for obtaining the laser light peak and the calibration method. This paper describes an elegant projective calibration method that obtains the best 2D to 3D point correspondences taking advantage of the invariance of the cross-ratio

*This research has been partially funded by the spanish project CYCYT TIC2003-08106-CO2-02.
e-mail: forest,qsalvi@eia.udg.es, enric.cabruja,marc.bigas@cnm.es

under collineations and a specially designed calibration target based on the shape of a complete quadrangle.

1. INTRODUCTION

The projective calibration of cameras rely on the identification of a good set of 2D to 3D point correspondences, which are used for obtaining **a)**the camera matrix P for single view geometry[1,2] , **b)**the fundamental matrix F for two view geometry[3,4] and **c)**the trifocal tensor T for three-view geometry[5,6] . The above problems are reduced to a parameter estimation problem, which can be solved with state-of-the-art minimisation techniques[7–11] either directly or iteratively. It is well known that the better the point correspondences match, the better the parameter estimation, and hence the system can be modelled more reliably. One of the contributions of this work is a method for obtaining the best 3D correspondence to previously chosen 2D points on the image. Since the 3D points used for calibration lie on the laser stripe, an explicit calibration of the camera is avoided and the whole camera-laser emitter system is modelled by a 4x3 matrix defined up to scale with 11 degrees of freedom, as stated by[12]Chen. However, the technique can also be used for camera calibration. The second contribution of this paper is the extension of Chen's method to systems in which the laser stripe scans the scene, while the camera does not vary its orientation relative to the object being scanned. A 4x3 matrix is obtained for each scanning calibration position and a function interpolation is used for every matrix parameter, in order to obtain a high scanning resolution. The method has been simulated for both angular and linear scanning, and an experimental linear scanning system has been implemented. In order to obtain the laser peak position, we developed our own peak detector. A comparative review of numerical peak detectors is analysed in[13] , and any of the peak detectors reported here would be suitable for integration with our calibration method. Besides, a review of calibration methods for three-dimensional laser scanners, so that the performance of the proposed method can be compared, is also detailed in[14] . The paper is structured as follows:

the next section briefly describes the previous work, with regard to the projective calibration of laser scanners. The proposed method for obtaining point correspondences is described in section 3, while section 4 shows how the projective method is used for scanning lasers. In section 5 we give the experimental results. The paper ends with conclusions and a short discussion on how the results could be improved.

2. PREVIOUS WORK

The geometric relation between two planes in projective space can be modelled by a 3x3 transformation matrix called *homography*. Chen and Kak[12] *borrowed* this projective result and used a homography for modelling the geometric relationship between the laser plane and the image plane. However, a homography relates 2D points on a plane to 2D points on a second plane and does not solve the process of mapping from 2D points to 3D points. With this aim, Chen demonstrated that a 3D coordinate system could be added to the laser plane, such that points on the laser plane expand naturally to 3D coordinates by adding a third component equal to zero to the 2D coordinates. Figure 1 shows a scheme of the above discussion, where $\{\mathbf{W}\}$ is the world or reference coordinate system, $\{\mathbf{I}\}$ is the image coordinate system, with units expressed in pixels, and $\{\mathbf{L}\}$ is the laser coordinate system. $\{\mathbf{L2}\}$ is a bi-dimensional coordinate system, where the x and y coincide with the x and y axis of $\{\mathbf{L}\}$. As shown in equation 1, the geometry of the whole system can be modelled by a 4x3 transformation ${}^{W}T_{I}$ with 11 degrees of freedom. This transformation allows the points on the laser plane to be mapped to 3D coordinates, with respect to $\{\mathbf{W}\}$.

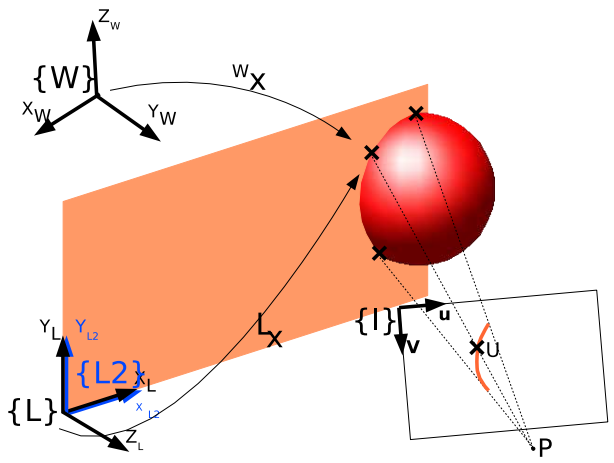

Figure 1. Geometric scheme of Chen & Kak's method.

$$\begin{bmatrix} x \\ y \\ z \\ w \end{bmatrix} = {}^{W}T_{L} \cdot {}^{L}T_{L2} \cdot {}^{L2}H_{I} \cdot \begin{bmatrix} u \\ v \\ 1 \end{bmatrix} = {}^{W}T_{L} \cdot \begin{bmatrix} 1 & 0 & 0 \\ 0 & 1 & 0 \\ 0 & 0 & 0 \\ 0 & 0 & 1 \end{bmatrix} \cdot$$
$$\cdot \begin{bmatrix} e_{11} & e_{12} & e_{13} \\ e_{21} & e_{22} & e_{23} \\ e_{31} & e_{32} & e_{33} \end{bmatrix} \cdot \begin{bmatrix} u \\ v \\ 1 \end{bmatrix} = \begin{bmatrix} t_{11} & t_{12} & t_{13} \\ t_{21} & t_{22} & t_{23} \\ t_{31} & t_{32} & t_{33} \\ t_{41} & t_{42} & t_{43} \end{bmatrix} \cdot \begin{bmatrix} u \\ v \\ 1 \end{bmatrix} = {}^{W}T_{I} \cdot \begin{bmatrix} u \\ v \\ 1 \end{bmatrix} \tag{1}$$

Reid[15] used the projective approach in order to calibrate the Oxford/NEL range finder on the Oxford AGV. In this work, and for the purpose of robot navigation, it was shown that only 8 degrees of freedom were required, instead of the 11 formerly stated. The Oxford/NEL range finder is a modification of the system proposed by Chen. It also consists in a camera and a laser emitter, but both the image and the laser stripe are reflected on a rotating mirror, so additional geometry is necessarily considered in the system modelling. Both of the previous works, required the pose of the scanner (camera-laser set) to be known precisely with respect to an arbitrary coordinate system, which makes reconstruction dependent on the values of the

position controllers. Hence, the scanner has to be mounted on a robot arm, as Chen suggested, or on a mobile robot. In both cases, significant inaccuracies may arise due to the positioning mechanics. Huynh[16] adopted the projective model in order to calibrate a fringe projection range finder. In this work, a different 4x3 transformation matrix is obtained for every fringe. The whole set of fringes is projected at the same time, so every light plane must be uniquely identified in order to set its relation to the corresponding 4x3 transform. Huynh proposed a method for obtaining point to point correspondences from known 3D points, based on the invariance of the cross-ratio. The 3D data for comparison were obtained using the SHAPE[17] scanner. Since a commercial scanner was used, the spatial point resolution is limited by the number of fringes this scanner is able to project. Improvement in performance can only be evaluated in terms of accuracy, since there is no possibility of measuring how fast or how robust it is in the presence of noise. Jokinen[18] used the projective relationship between a laser plane and the image plane as a starting point for refining a laser stripe scanner calibration.

3. OBTAINING POINT CORRESPONDENCES

Any set of four non-aligned points A, B, C, D on the plane can be joined pairwise by six distinct lines as shown in figure 2a. This figure is called the *Complete Quadrangle* and exhibits several useful properties in computer vision applications[19] . In this work, points A, B, C, D, F and G are used in order to generate 3D points for calibration and their correspondences on the image plane.

3.1. The cross-ratio

The cross-ratio of a pencil of four lines can be defined by the four points of intersection of a fifth line not pertaining to the pencil. If these four collinear points are labelled A, B, C and D, the cross-ratio can be defined by equation 2. It can be proved that the cross-ratio is invariant under projective transformations of points A, B, C and D. Figure 2b shows such a situation. Since the

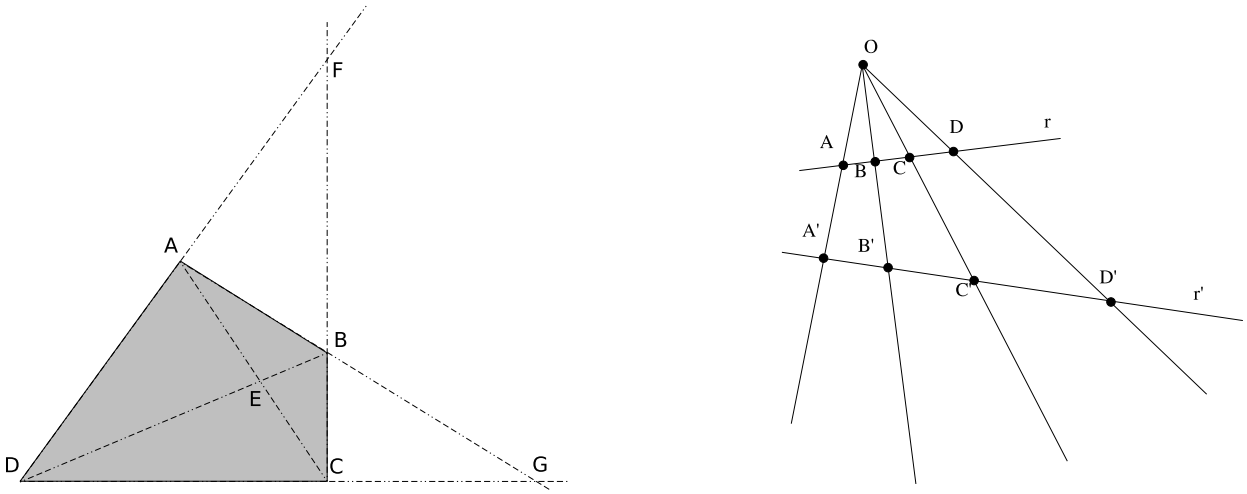

Figure 2. The complete quadrangle (a) and the invariance of the cross-ratio (b).

cross-ratio is a ratio of ratios of lengths, it is straightforward to express the line equations in their parametric forms. In addition, if the line equations are computed using the first and the fourth points, i.e. points A and D , according to equation 3, $\lambda = 0$ yields $r = A$, $\lambda = \overline{AB}$ yields $r = B$ and so forth. Hence, using the parametric forms of the line equations in this way, $\lambda_{1..3}$ can be defined with the values: $\lambda_1 = \overline{AB}$, $\lambda_2 = \overline{AC}$ and $\lambda_3 = \overline{AD}$. According to these definitions, the cross-ratio of points A,B,C and D can be computed as shown in equation 4, which is the form that will be used in our approach. In addition, if the cross-ratio and only 3 of the 4 points are known, equation 5 can be used for obtaining the coordinates of the fourth point.

$$Cr\{A, B; C, D\} = \frac{\overline{AC} \cdot \overline{BD}}{\overline{AD} \cdot \overline{BC}} \quad \text{where } \overline{XY} \text{ is the distance between points X and Y} \tag{2}$$

$$r = \lambda \cdot \frac{D - A}{\|D - A\|} + A \tag{3}$$

$$k = \frac{\lambda_2 \cdot (\lambda_3 - \lambda_1)}{\lambda_3 \cdot (\lambda_2 - \lambda_1)} \tag{4}$$

$$\lambda'_2 = \frac{k \cdot \lambda'_3 \cdot \lambda'_1}{(k-1) \cdot \lambda'_3 + \lambda'_1} \tag{5}$$

3.2. Points on the upper and lower edges

Figure 3 shows how the four lines defined by point **F** and points A, P_A, B, and G respectively, configure a pencil of lines. Hence it is straightforward to obtain their cross-ratio, provided that point P_A is known. However, P_A is an unknown world 3D point, with only the line that contains it being known, that is, only points A, B, and G are known. Nevertheless, if we look at the image, it can be seen that points A', P'_A, B' and G' are all known. Since the geometric relation between points A to G and points A' to G' is projective, the cross-ratio can be computed with points A' to G' and its value can be used for computing the coordinates of point P_A. The same procedure can be adopted between points D to G and D' to G'. By repeating the process for different positions of the laser stripe, it can be seen that a set of correspondences $P_A \Leftrightarrow P'_A$ and $P_B \Leftrightarrow P'_B$ can be established with high accuracy.

3.3. Points on the laser stripe

The estimation of the 4x3 transformation ${}^{W}T_I$, which maps points on the image plane (${}^{I}P$) to points on the laser plane (${}^{W}P$), is performed from point to point correspondences. In subsection 3.2, we explained a method for obtaining the intersection points of the laser plane with the upper and lower lines of the calibration target. However, only two points define the laser stripe for each depth, as shown in figure 4a. It is reasonable to think, however, that the more points per stripe are obtained, the better the parameter estimation of ${}^{W}T_I$ is. Looking back to figure 3, it is clear that the cross-ratio of points F', A', D' and an arbitrary 2D point P'_L between A' and D' can be obtained. Since points F, A and D are known, the previously computed cross-ratio can be used for calculating the coordinates of the 3D point P_L corresponding to P'_L. This process is depicted in figure 4b, where the points on the line $A'D'$ are called P'_L. It is clear that a pencil of lines L'_T can be defined between point G' and points P'_L, and that these

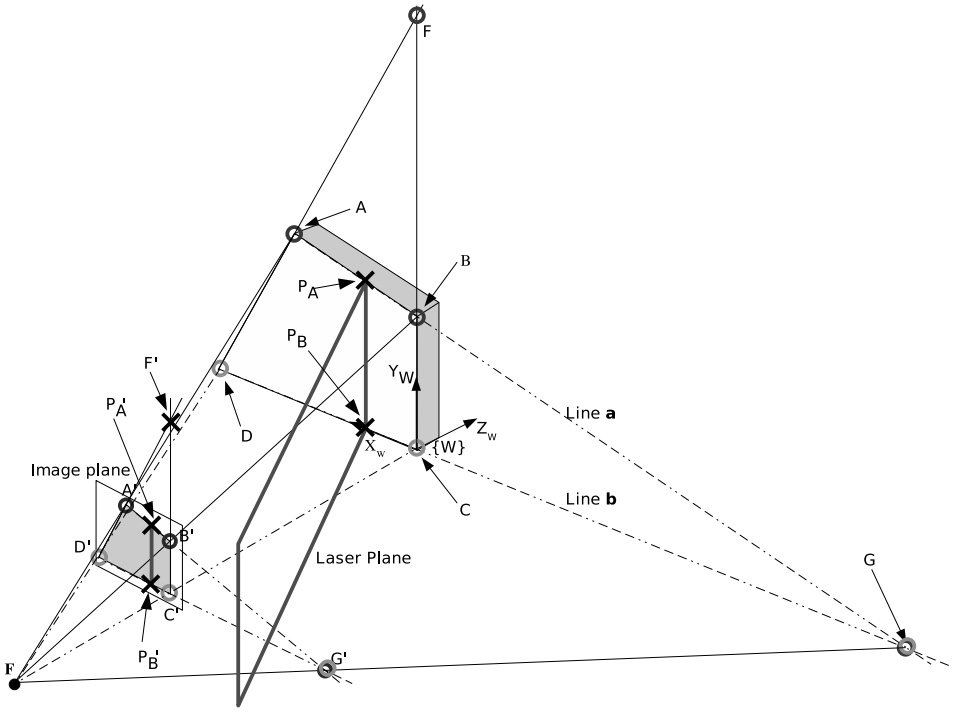

Figure 3. The cross-ratio and the complete quadrangle.

lines define a set of intersection points P'_R on the line $B'C'$. Now, for each of the lines of the pencil L'_T, the intersection with the laser stripe P'_S can be obtained, and hence, the cross-ratio between point G', P'_R, P'_S and P'_L can be calculated. Finally, since the 3D points G, P_R and P_L are known, the value of the cross-ratio can be used in order to obtain the set of 3D points P_S laying on the laser stripe.

3.4. Validation

In order to validate the quality of the 3D point generation, a plane equation has been fitted using TLS[†], to the points obtained for each laser plane position. Table 1 shows the orientation of the laser plane by using the angles α, β and γ, of the direction cosines of the plane's normal vector. The position of the plane is shown as well, in the form of ΔX_w, which is the separation

[†]Total Least Squares

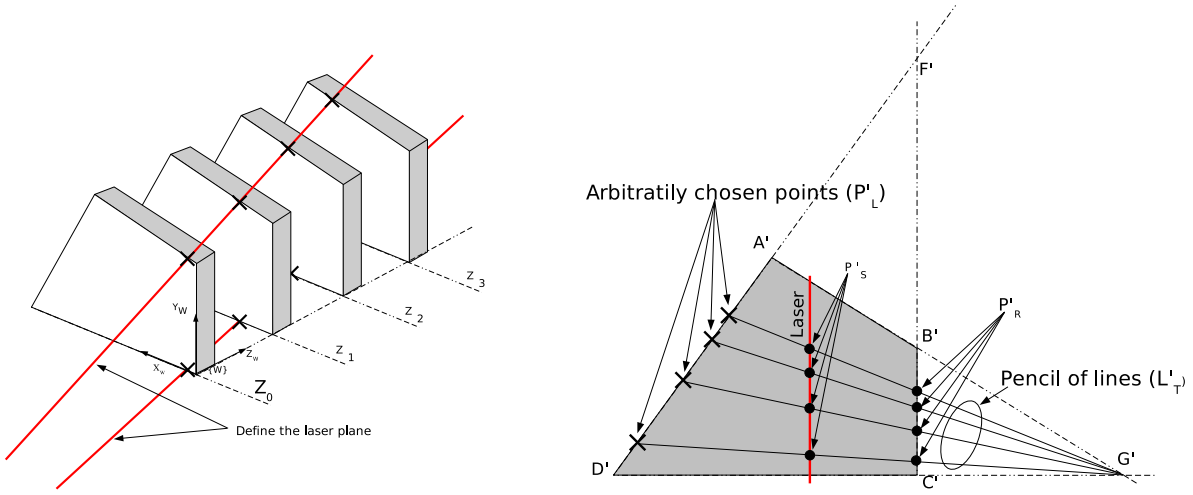

(a) (b)

Figure 4. The laser plane defined by upper and lower points (a) and Point generation (b).

Table 1. Fit of a plane equation to each of the laser plane positions.

Eq.	**Values ± error (3σ)**		
	added σ=0	added σ=1	added σ=2
α	161.2824±0.0033^o	161.3082±0.0385	161.2647±0.1418
β	90.0715±0.0092^o	90.0492±0.2081	90.0733±0.1128
γ	71.2826±0.0096^o	71.3084±0.1140	71.2659±0.4169
ΔX_w	4.0406±0.0452 mm	4.0369±0.4154	4.0034±0.7420

between laser positions. In order to see how Gaussian noise influences the point generation, extra noise with σ=1 and σ=2 pixels has been added, and the results of the plane fitting are displayed in table 1. It is worth noting that ΔX_w has been chosen to be 4mm in our position controller. However, an offset of 40μm and an error of 45μm are introduced by the mechanics and the controller accuracy, in the case of added σ=0. As can be seen in table 1, the plane orientation is very stable for low noise values, and does not perform badly for very high noise levels. These values show that the point generation algorithm is a good choice for accurate point correspondence generation.

4. CALIBRATION

Once the point correspondences have been identified for each stripe position, the parameters of the 2D to 3D mapping must be estimated. Equation 6 shows the relationship between points on the image plane ${}^{I}[u, v, 1]^{T}$ with 3D points ${}^{W}[sX, sY, sZ, s]^{T}$ on the laser plane.

$$\begin{bmatrix} sX \\ sY \\ sZ \\ s \end{bmatrix} = \begin{bmatrix} t_{11} & t_{12} & t_{13} \\ t_{21} & t_{22} & t_{23} \\ t_{31} & t_{32} & t_{33} \\ t_{41} & t_{42} & t_{43} \end{bmatrix} \cdot \begin{bmatrix} u \\ v \\ 1 \end{bmatrix} \tag{6}$$

Obviously, the parameters t_{11} to t_{34} should be estimated as precisely as possible, in order to maximise the accuracy of the reconstruction. According to equation 6, the expressions for sX, sY, sZ and s are obtained and shown in equation 7.

$$\begin{aligned} sX &= t_{11} \cdot u + t_{12} \cdot v + t_{13} \\ sY &= t_{21} \cdot u + t_{22} \cdot v + t_{23} \\ sZ &= t_{31} \cdot u + t_{32} \cdot v + t_{33} \\ s &= t_{41} \cdot u + t_{42} \cdot v + t_{43} \end{aligned} \tag{7}$$

Arranging the terms and grouping, a homogeneous system of three equations with 12 unknowns (t_{11} to t_{43}) is obtained, as shown in equation 8.

$$\begin{aligned} t_{11} \cdot u + t_{12} \cdot v + t_{13} - t_{41} \cdot u \cdot X - t_{42} \cdot v \cdot X - t_{43} \cdot X = 0 \\ t_{21} \cdot u + t_{22} \cdot v + t_{23} - t_{41} \cdot u \cdot Y - t_{42} \cdot v \cdot Y - t_{43} \cdot Y = 0 \\ t_{31} \cdot u + t_{32} \cdot v + t_{33} - t_{41} \cdot u \cdot Z - t_{42} \cdot v \cdot Z - t_{43} \cdot Z = 0 \end{aligned} \tag{8}$$

It can be seen that one single point correspondence contributes with 3 equations in 12 unknowns, with only their ratio being significant. Hence, at least 4 non-collinear points are needed in order to find the 12 parameters. However, due to the presence of noise in the measurement, it is

reasonable to transform the problem into a least-squares-type parameter estimation problem, by using more than four noisy point correspondences. Rewriting equation 8 in matrix form, equation 9 is obtained, which is the expression of a parameter estimation problem, that can be solved by computing the vector θ that minimises some cost function of the matrix equation $A \cdot \theta = 0$. A good estimation using TLS techniques can be found by computing the eigenvector corresponding to the smallest eigenvalue of matrix $A^T \cdot A$. In addition, the iterative solution proposed by Van den Hengel[20] , the Fundamental Numerical Scheme (FNS), has been tested for estimating the ${}^{W}T_{I}$ parameters.The estimation accuracy of FNS is comparable to that of the Levenberg-Marquardt algorithm, but the rate of convergence is faster. However, FNS requires a good approximation of the covariance matrix for each data sample, which was not available in our experiments. In this case, FNS performed like TLS, but notably slower.

$$\begin{bmatrix} \vdots & & \vdots & & \vdots & & \vdots & & \vdots \\ u_i & v_i & 1 & 0 & 0 & 0 & 0 & 0 & 0 & -u_i \cdot X_i & -v_i \cdot X_i & -X_i \\ 0 & 0 & 0 & u_i & v_i & 1 & 0 & 0 & 0 & -u_i \cdot Y_i & -v_i \cdot Y_i & -Y_i \\ 0 & 0 & 0 & 0 & 0 & 0 & u_i & v_i & 1 & -u_i \cdot Z_i & -v_i \cdot Z_i & -Z_i \\ \vdots & & \vdots & & \vdots & & \vdots & & \vdots \end{bmatrix} \cdot \begin{bmatrix} t_{11} \\ t_{12} \\ t_{13} \\ t_{21} \\ t_{22} \\ t_{23} \\ t_{31} \\ t_{32} \\ t_{33} \\ t_{41} \\ t_{42} \\ t_{43} \end{bmatrix} = \begin{bmatrix} \vdots \\ 0 \\ 0 \\ 0 \\ \vdots \end{bmatrix} \quad (9)$$

With the parameter estimation for each stripe position, a *set* of ${}^{W}TI$ is obtained. In the case of linear scanning, a line can be fitted to the set of parameters corresponding to each matrix

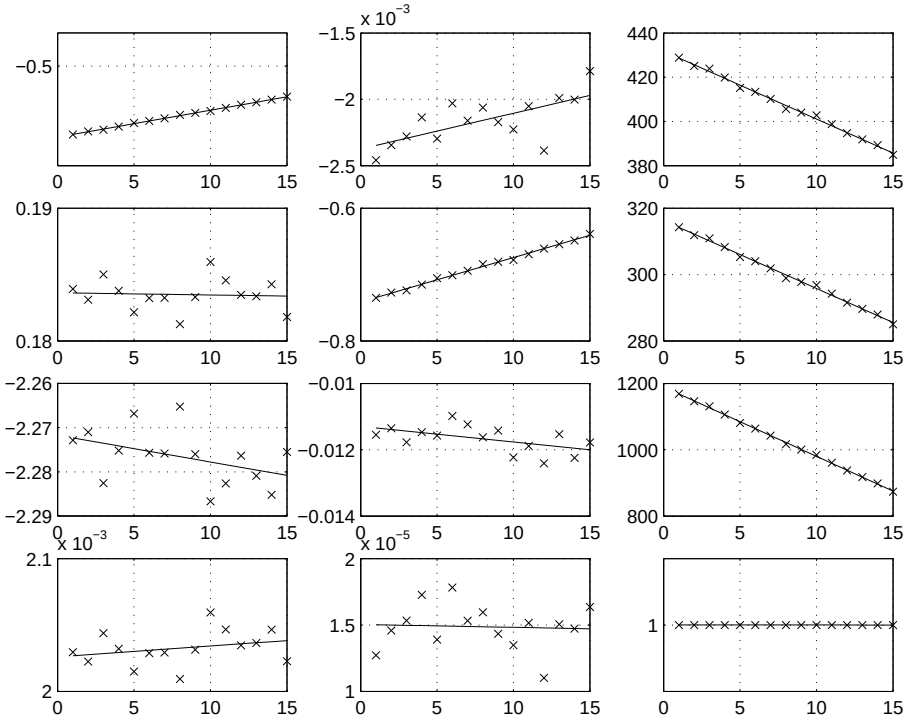

Figure 5. Plots of the values of ${}^{W}T_{I}$ and the lines fitted.

component. The case of angular scanning has not been tested in this work, but simulation results show that, instead of a line, a 2nd order function can be fitted. Figure 5 shows the values of the set of ${}^{W}T_{I}$ and the lines which have been fitted to them. Note that the parameters have been scaled so that ${}^{W}T_{I34}$ is 1, in order to facilitate the comparison between the matrices.

5. EXPERIMENTAL RESULTS

Once the set of ${}^{W}T_{I}$ matrices has been obtained, it is straightforward to test how good the calibration method is. To this end, two experiments have been undertaken. The former consists in reconstructing the 2D points (${}^{I}\hat{P}$) obtained from the calibration images, as explained in section 3. In the ideal case of computers having infinite precision and the stripe images being taken in the absence of noise, the difference between the 3D points obtained by this procedure

($^W P$) and the 3D points obtained by the complete quadrangle method ($^W \hat{P}$) is zero. However, computer operations exhibit limited performance due to their limited accuracy. Furthermore, image sensors are subject to electrical noise during the imaging process, and the mechanics used for scanning the laser stripe are subject to position inaccuracies. Hence, due to these diverse noise sources, reconstructing the calibration planes is subject to errors, which are displayed as offsets and discrepancy between $^W \hat{P}$ and $^W P$, as displayed in figure 6. The narrower error interval corresponds to the values without added Gaussian noise, the middle and the wider values correspond to added noise of σ=1 pixel and σ=2 pixels, respectively. Figure 7b shows a scheme of the system which was built in our lab for testing the calibration algorithm. The laser emitter is a semiconductor diode which outputs light at 1mW peak power with λ=650nm. In addition, a cylindrical lens is provided with the laser housing so that it is capable of projecting a plane of light with an 85^o aperture and 1mm width. The camera optics focal length is 25mm, and an optical bandpass filter with BW=10nm and λ_c=650nm is provided. The image resolution we have used is standard VGA (640x480 pixels) with 8 bit grey level. The distance of the object under consideration is about 1200mm, while the laser incidence angle with respect to the optical axis of the camera is approximately 18.5^o.

The second experiment consists in scanning a well known object with simple geometric features. We chose a cylinder for this object with ø=73.30mm, measured with a digital caliper with $\pm$ 20μm accuracy. The 3D reconstruction of such cylinder is shown in figure 7a. In order to extract the diameter, a TLS scheme has been used to fit a cylinder to the reconstructed data, and the data has been added Gaussian noise with σ=0.4 to 2 pixels. The results are summarised in table 2, and the measurements have been taken at a distance of 1100mm.

6. CONCLUSIONS

A novel and elegant method for obtaining highly accurate 2D to 3D point correspondences for calibration has been explained. In this work, we used it for the calibration of a laser 3D

Table 2. Reconstructed radius of the fitted cylinder with different noise levels.

Added σ	Diameter ø	% Rel. error
0	73.52	0.3
0.4	73.16	0.2
0.8	72.07	1.7
1	71.14	3
1.4	69.21	6
1.8	66.90	9.6
2	65.38	12.1

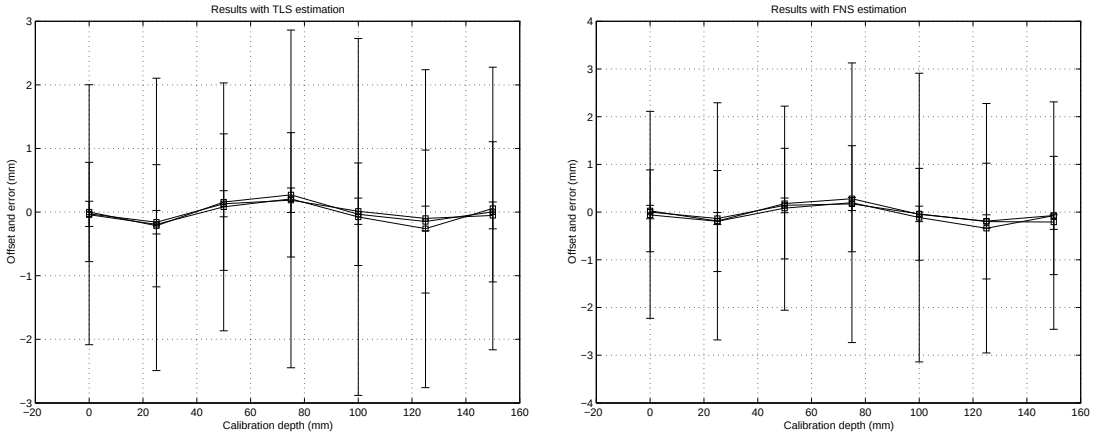

(a) (b)

Figure 6. Errors in the reconstruction of the calibration planes using (a) TLS and (b) FNS methods.

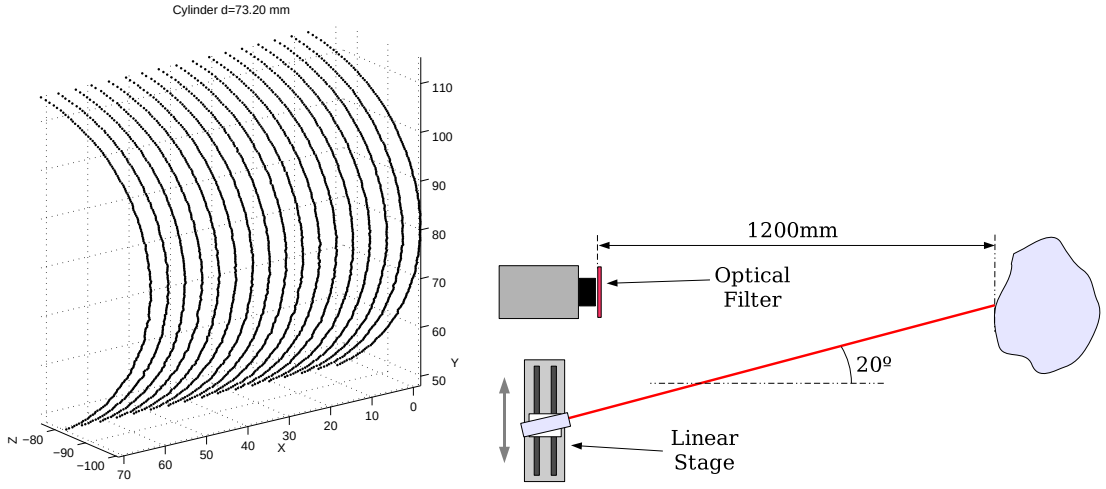

(a) (b)

Figure 7. Reconstruction of a cylinder (a) and the lab scanner (b).

scanner, although the method is also valid for standard camera calibration. In addition, the projective calibration approach for 3D laser scanners has been extended for use in *scanning laser, static camera*-type systems. One of the most powerful features of the projective approach is that no physical model of the system is necessary, since the whole geometry is contained in a single matrix. This feature has been kept in our proposal, since the whole system geometry is contained in a *set* of matrices. The experiments undertaken in our laboratory facilities exhibits very good results considering the components used for configuring the set-up. It is clear that the most influential issue in this calibration algorithm is the parameter estimation optimisation algorithm. In order to improve the performance, the parameter estimation using both FNS and Levenberg-Marquardt algorithms has been carried out. However, the performance of both FNS and Levenberg-Marquardt is significantly affected by a good estimation of the covariance matrix for each observation. Since the system calibration is done under controlled conditions, the estimation of the covariance matrix can be obtained from successive samples of the same laser position for different lighting conditions. It is the belief of the authors that the accuracy can be improved by at least one order of magnitude with an optimal parameter estimation.

REFERENCES

1. R. Hartley and A. Zisserman, *Multiple view geometry*, Cambridge University Press, 2000.
2. J. Salvi, X. Armangué, and J. Batlle, "A comparative review of camera calibrating methods with accuracy evaluation," *Pattern Recognition* **35**, pp. 1617–1635, August 2002.
3. G. T. O.D. Faugeras, "The calibration problem for stereo," in *Proceedings of the 1986 IEEE Computer Vision and Pattern Recognition*, pp. 15–20, 1986.
4. X. Armangué and J. Salvi, "Overall view regarding fundamental matrix estimation," *Image and Vision Computing* **21**(2), pp. 205–220, 2003.
5. O. Faugeras, *Three-Dimensional Computer Vision: A Geometric Viewpoint*, The MIT Press, 1993.

6. O. Faugeras and T. Papadopoulo, "Grassmann-cayley algebra for modeling systems of cameras and the algebraic equations of the manifold of trifocal tensors," Rapport de recherche 3225, INRIA, July 1997.
7. W. Chojnacki, M. J. Brooks, A. van den Hengel, and D. Gawley, "On the fitting of surfaces to data with covariances," *IEEE Transactions on Pattern Analysis and Machine Intelligence* **22**(11), pp. 1294–1303, 2000.
8. W. Chojnacki, M. J. Brooks, A. van den Hengel, and D. Gawley, "A fast mle-based method for estimating the fundamental matrix," in *Proceedings of the International Conference on Image Processing*, **2**, pp. 189–192, 2001.
9. W. Chojnacki, M. J. Brooks, A. van den Hengel, and D. Gawley, "Fns and heiv: relating two vision parameter estimation frameworks," in *Proceedings of the 12th International Conference on Image Analysis and Processing*, pp. 152 – 157, 2003.
10. K. Kanatani, N. Ohta, and Y. Kanazawa, "Optimal homography computation with a reliability measure," *IEICE Transactions on Informatics and Systems* **E38-D**(7), pp. 1369–1374, 2000.
11. Y. Leedan and P. Meer, "Heteroscedastic regression in computer vision: Problems with bilinear constraint," *International Journal of Computer Vision* **37**(2), pp. 127–150, 2000.
12. C. Chen and A. Kak, "Modeling and calibration of a structured light scanner for 3-d robot viison," in *Proceedings of the IEEE conference on robotics and automation*, pp. 807–815, IEEE, 1987.
13. E. Trucco, R. Fisher, A. Fitzgibbon, and D. Naidu, "Calibration, data consistency and model acquisition with a 3-d laser striper," *International Journal of Computer Integrated Manufacturing* **11**(4), pp. 292–310, 1998.
14. J. Forest and J. Salvi, "A review of laser scanning three-dimensional digitisers," in *Intelligent Robots and Systems, 2002*, pp. 73–78, IEEE/RSJ, 2002.
15. I. D. Reid, "Projective calibration of a laser-stripe range finder," *Image and Vision Computing* **14**, pp. 659–666, 1996.
16. D. Q. Huynh, "Calibration of a structured light system: a projective approach," in *Proceedings of the 1997 IEEE Computer Society Conference on Computer Vision and Pattern Recognition*, IEEE, ed., pp. 225–230, 1997.

17. B. Alexander and K. Ng., "3d shape measurement by active triangulation using an array of coded light stripes," in *Proceedings of the SPIE: Optics, Illumination and Image Sensing for Machine Vision II*, **850**, pp. 199–209, 1987.

18. O. Jokinen, "Self-calibration of a light striping system by matching multiple 3-d profile maps," in *Proceedings of the Second International Conference on 3-D Digital Imaging and Modeling*, pp. 180 – 190, 1999.

19. R. Mohr and B. Triggs, "Projective geometry for image analysis.," tech. rep., INRIA, 1996. A tutorial given at ISPRS in Vienna 1996.

20. A. V. den Hengel, M. Brooks, W. Chojnacki, and D. Gawley, "Approximated maximum likelyhood estimation and the fundamental numerical scheme," tech. rep., University of Adelaide (Australia), 2000.